ADVANCED FUNCTIONAL MATERIALS
www.afm-journal.de

Effect of Non-Chlorinated Mixed Solvents on Charge Transport and Morphology of Solution-Processed Polymer Field-Effect Transistors

Wen-Ya Lee, Gaurav Giri, Ying Diao, Christopher J. Tassone, James R. Matthews, Michael L. Sorensen, Stefan C. B. Mannsfeld, Wen-Chang Chen, Hon H. Fong, Jeffrey B.-H. Tok, Michael F. Toney, Mingqian He, and Zhenan Bao**

Using non-chlorinated solvents for polymer device fabrication is highly desirable to avoid the negative environmental and health effects of chlorinated solvents. Here, a non-chlorinated mixed solvent system, composed by a mixture of tetrahydronaphthalene and *p*-xylene, is described for processing a high mobility donor-acceptor fused thiophene-diketopyrrolopyrrole copolymer (PTDPPTFT4) in thin film transistors. The effects of the use of a mixed solvent system on the device performance, e.g., charge transport, morphology, and molecular packing, are investigated. *p*-Xylene is chosen to promote polymer aggregation in solution, while a higher boiling point solvent, tetrahydronaphthalene, is used to allow a longer evaporation time and better solubility, which further facilitates morphological tuning. By optimizing the ratio of the two solvents, the charge transport characteristics of the polymer semiconductor device are observed to significantly improve for polymer devices deposited by spin coating and solution shearing. Average charge carrier mobilities of 3.13 $cm^2 V^{-1} s^{-1}$ and a maximum value as high as 3.94 $cm^2 V^{-1} s^{-1}$ are obtained by solution shearing. The combination of non-chlorinated mixed solvents and the solution shearing film deposition provide a practical and environmentally-friendly approach to achieve high performance polymer transistor devices.

1. Introduction

Conjugated polymers have long been considered as promising alternative candidates to amorphous silicon as the semiconductor in field-effect transistors (FETs). This is because they are easily solution processed, have excellent mechanical properties and can be deposited at relatively low substrate temperatures (below 200 °C).[1–4] Large scale and low cost polymer-based electronic devices can be fabricated by solution deposition methods, such as roll-to-roll printing and spin-coating. However, polymer-based FETs usually exhibit lower charge carrier mobilities compared to devices based on small organic molecules. This is primarily due to the presence of amorphous regions, which may limit charge transport.[5] In recent years, several high-performance polymeric materials have been reported with charge carrier mobilities exceeding 1 $cm^2 V^{-1} s^{-1}$, for example, poly(bis-alkylthiophenyl thienothiophene) (PBTTT),[6] poly(cyclopentadithiophene-benzothiadiazole),[7,8] isoindigo-based polymers[9,10] and diketopyrrolopyrrole (DPP)-based polymers.[11–21] Of particular interest is a report by Ong and Liu describing a breakthrough in achieving charge carrier mobility with a value as high as 10 $cm^2 V^{-1} s^{-1}$ from poly(dithienylthieno[3,2-b]thiophene-DPP).[12] Together, these results indicate that the performance of conjugated polymers can be rendered comparable to, or better than, traditional amorphous Si-based transistors. However, most high-mobility polymer FETs are processed with halogenated solvents, for instance, chloroform, chlorobenzene and dichlorobenzene, despite their health hazard and detrimental environmental impact. Furthermore, the usage of chlorinated solvents in industry is highly regulated, which requires special setups to prevent exposure to toxic solvent vapor and expensive halogenated solvent recovery systems to protect the environment. Therefore, non-chlorinated solvent processing of high-performance polymer devices is important for large-scale production of polymer FETs.

Dr. W.-Y. Lee, G. Giri, Dr. Y. Diao, Dr. J. B.-H. Tok, Prof. Z. Bao
Department of Chemical Engineering
Stanford University
381 North-South Mall, Stanford, CA 94305, USA
E-mail: zbao@stanford.edu
Dr. C. J. Tassone, Dr. S. C. B. Mannsfeld, Dr. M. F. Toney
Stanford Synchrotron Radiation Laboratory
2575 Sand Hill Rd, Menlo Park, CA 94025, USA
Dr. J. R. Matthews, M. L. Sorensen, Dr. M. He
Corning Incorporated
SP-FR-06–1, Corning, NY 14831, USA
E-mail: hem@corning.com
Prof. W.-C. Chen
Department of Chemical Engineering
National Taiwan University
Taipei 106, Taiwan
Prof. H. H. Fong
Shanghai Jiao Tong University
Comprehensive Laboratory Building
Room 2–603, 800 DongChuan Rd., Shanghai 200240, China

DOI: 10.1002/adfm.201303794

Selection of appropriate solvents to optimize the electrical performance of polymer FETs is a topic of intense investigation. Specifically, both the boiling point and Hansen solubility parameter of the employed solvents are important considerations.[22,23] Sirringhaus and coworkers reported that polymer thin films cast from high boiling point solvents, for example, trichlorobenzene, resulted in a higher charge carrier mobility for poly(3-hexyl thiophene) (P3HT) compared to those cast from low boiling point solvents.[22] This was attributed to the slow evaporation of the high boiling point solvent, thus facilitating the formation of more ordered thin films. However, boiling point is not the only factor affecting the ordering of polymer thin films. The solubility behavior of polymers in various solvents should also be considered. By selecting appropriate solvents based on polymer solubility, the morphology of P3HT can be changed to a highly crystalline nanofiber network.[23–25] Furthermore, our group has found that morphological connectivity of nanofibrillar crystalline domains and crystalline orientation of the π–π stacking plane also play important roles on charge transport in polymer films.[23] The above examples indicate that both the boiling point and solubility parameter of processing solvents will impact microstructures of polymer semiconductor films, which subsequently influence the charge transport behavior of these polymers.

In addition to solvent selection, the solution deposition method is also important to control the organic semiconductor film crystallinity and morphology. Several solution processing methods, for example, droplet-pinned crystallization,[26,27] spin coating,[28] zone casting,[29] and solution shearing,[30–34] have been demonstrated. Among these methods, solution shearing is a proven facile approach to fabricate high-performance FETs.[17,30–35] In this approach, a small volume of organic semiconductor solution is sandwiched between two substrates held at an elevated substrate temperature. With the bottom substrate stationary, the top substrate is pulled at a specific speed. The crystallization of organic semiconducting materials can be controlled by simply changing the substrate temperature and shearing speed in addition to solution characteristics. The solution-sheared films were often observed to exhibit higher charge carrier mobility, as compared to equivalent devices prepared from spin coating.[17] Additionally, we have observed that 6,13-bis(triisopropylsilylethynyl) pentacene (TIPS-pentacene) films by solution shearing exhibited a hole mobility as high as 4.6 $cm^2\ V^{-1}\ s^{-1}$. The solution shearing approach results in the formation of meta-stable, strained packing structures and in some cases an enhancement of charge transfer integral between π–π stacked molecules, thus benefiting charge transport.[31] Recently, the Oh and Yang groups have employed the solution shearing method to enhance device performance of polymer thin-film transistors,[17] suggesting solution shearing is also suitable to optimize the crystalline structure and morphology of polymer films. However, the influence of solvent quality on solution sheared polymer film is yet to be studied.

We have recently reported a high-mobility donor-acceptor tetrathienoacene-DPP based copolymer (PTDPPTFT4) that has long, linear alkyl side chains (**Figure 1**a).[36] This polymer exhibited a hole mobility as high as 2.1 $cm^2\ V^{-1}\ s^{-1}$. Furthermore, the long $C_{17}H_{35}$ alkyl side chains provided good solubility in commonly used non-chlorinated solvents, for example, toluene, xylene, and tetrahydronaphthalene (THN), suggesting that this semiconducting material may be suitable for solution processing from non-chlorinated solvents. This polymer also showed an apparent bi-modal molecular weight distribution as observed using Gel Permeation Chromatography (GPC) at moderate temperatures, even when trichlorobenzene was used as an eluent. We attributed this to its strong inter-chain interaction, which resulted in the aggregation of polymer chains in solution. Such aggregation may result in the formation of rough interfaces between aggregates in films, hence forming defects which subsequently suppress charge transport. On the other hand, aggregation may also induce an ordered self-assembled structure, thus enhancing charge transport. Hence, it is of interest to control polymer aggregation in solution to facilitate optimized electrical properties of polymer FETs.

Here, we report high-mobility polymer FETs by using a non-chlorinated mixed-solvent system of *p*-xylene and THN. Specifically, the ratios of these two solvents are optimally controlled to improve the performance of PTDPPTFT4-based FETs. We note that xylene has previously been used to promote polymer aggregation and enhance photovoltaic efficiency in solar cells.[37] In our investigation, we also observed that *p*-xylene is more prone to induce the gelation of polymer chains than THN. The chemical structure of the polymer (PTDPPTFT4) and the solution-shearing configuration are shown in Figure 1a,b. The morphology, crystalline orientation and electrical properties of PTDPPTFT4 polymer thin films are optimized by adding an appropriate amount of *p*-xylene into a solution of pre-dissolved PTDPPTFT4 in THN. We observed a charge carrier mobility of the PTDPPTFT4 FET as high as 3.94 $cm^2\ V^{-1}\ s^{-1}$ through using the mixed solvents and depositing the film by a solution-shearing process.[30]

2. Results and Discussion

2.1. Absorption Spectra Characterizations

The aggregation behavior of PTDPPTFT4 upon adding *p*-xylene to its THN solution was monitored by solution UV/Vis spectroscopy, as shown in Figure 1c. To obtain strong UV absorption, we prepared a high concentration solution (0.2 mg mL^{-1}), PTDPPTFT4 exhibited two absorption bands with two maxima at 430 nm and 807 nm. The absorption band at longer wavelength is attributed to intramolecular charge transfer between the donor and acceptor moieties in the polymer backbone. The intensity of the absorption peak at 807 nm increased with the amount of *p*-xylene added. The absorption peak increased from 1.26 A in 0% *p*-xylene to 1.46 A in 100% *p*-xylene. This may be attributed to the formation of aggregates. THN commonly showed good solubility for conjugated polymers due to its Hansen solubility parameter (δ_D: 19.6 $MPa^{1/2}$) close to many conjugated organic molecules and polymers, ex. thiophene (δ_D: 18.9 $MPa^{1/2}$), DPP-based derivative (DPP(TBFu)$_2$) (δ_D: 19.3 $MPa^{1/2}$), poly(cyclopentadithiophene-benzothidiazole) (PCPDTBT) (δ_D: 19.6 $MPa^{1/2}$) and PCBM (δ_D: 20.2 $MPa^{1/2}$).[38,39] As compared to THN, *p*-xylene is better at solvating the long

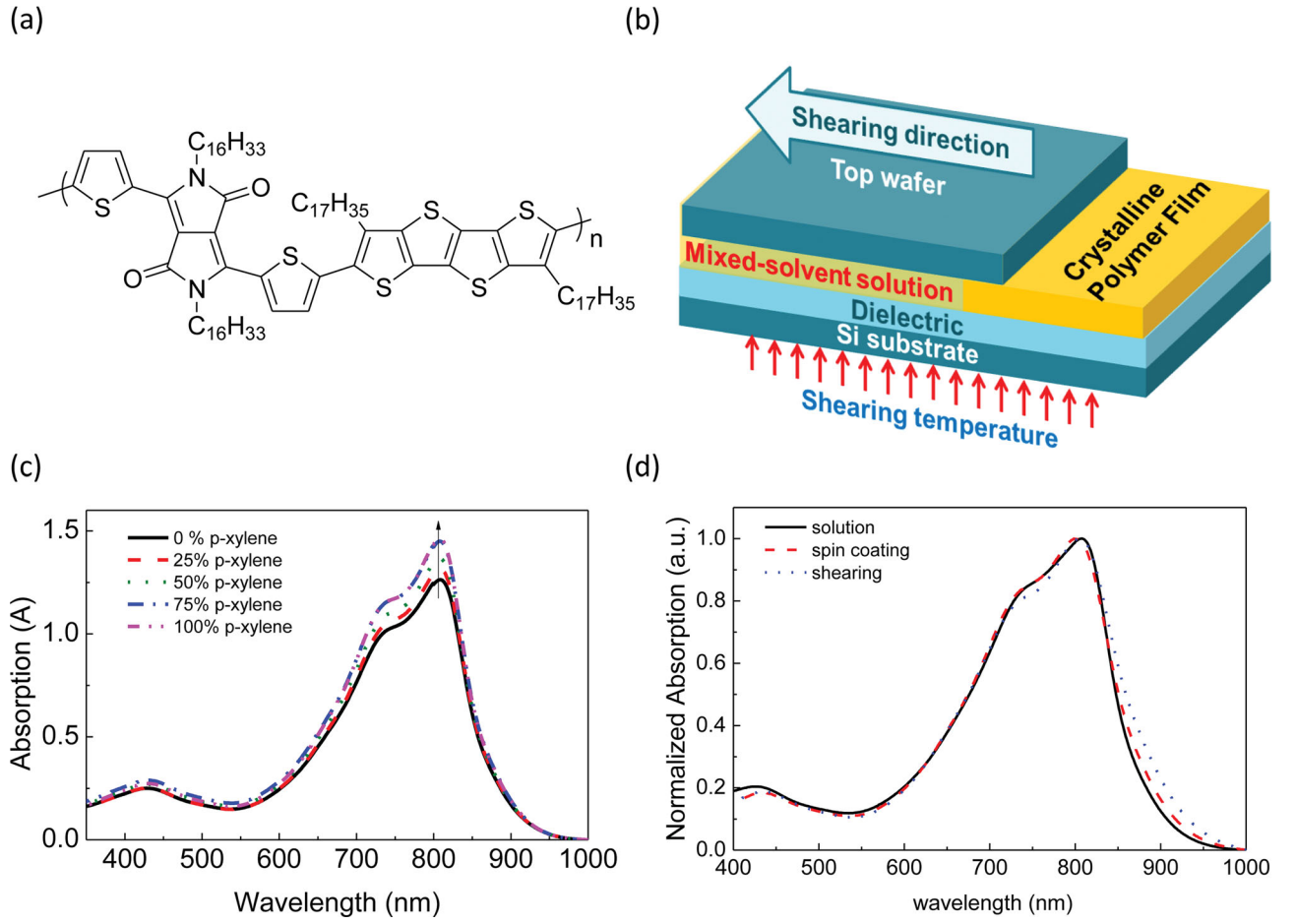

Figure 1. a) Chemical structure of PTDPPTFT4. b) Solution shearing configuration. c) UV-vis spectra of the mixed-solvent ratios (0, 25, 50, 75, 100% *p*-xylene in THN). d) UV-vis spectra of solution and thin-film states made from 25% *p*-xylene solution.

alkyl chains, because the Hansen solubility parameter of *p*-xylene (δ_D: 17.9 $MPa^{1/2}$) is close to that of the hexadecyl and heptadecyl side chains (16.4 $MPa^{1/2}$). Therefore, with increasing ratio of *p*-xylene, the high miscibility between *p*-xylene and the side chains may be beneficial to extend the alkyl chains and induce the self-assembly of polymer chains. Figure 1d shows the UV-vis spectra of the solution, spin-coated and solution-sheared thin films. There is a slight red shift of the absorption edge from solution to spin-coated to solution-sheared film, indicating increased aggregation of polymer chains. In addition to UV-vis spectra, we also measured photoluminescence spectra of these polymer solutions (Figure S1, Supporting Information). However, unfortunately, the intensity of the near-IR photoluminescence spectra is quite weak. Therefore, it is difficult to observe the change of polymer aggregation from these photoluminescence spectra.

Table 1. Summary of the electrical properties of PTDPPTFT4 FETs using different mixed-solvent ratios. These samples were prepared at the optimum deposition temperature.

Process	*p*-Xylene (%)	Mobility^{MAX} [$cm^2\ V^{-1}\ s^{-1}$]	Mobility ^{Avg} [$cm^2\ V^{-1}\ s^{-1}$]	on/off^{Avg}	$V_{th}{}^{Avg}$ [V]
spin coating	0	1.70	1.36 ± 0.24	$(3 \pm 2) \times 10^5$	-9 ± 3
	25	2.53	2.20 ± 0.28	$(2 \pm 1) \times 10^6$	-18 ± 1
	50	1.14	1.03 ± 0.08	$(4 \pm 3) \times 10^5$	-3 ± 3
	75	1.16	1.05 ± 0.20	$(6 \pm 4) \times 10^5$	-6 ± 3
	100	0.91	0.89 ± 0.18	$(4 \pm 3) \times 10^5$	-7 ± 2
solution shearing	0	3.12	2.76 ± 0.29	$(3 \pm 2) \times 10^3$	-19 ± 4
	25	3.94	3.13 ± 0.55	$(2 \pm 1) \times 10^6$	-15 ± 6
	50	2.89	2.21 ± 0.55	$(2 \pm 1) \times 10^4$	-13 ± 7
	75	2.84	2.08 ± 0.73	$(2 \pm 1) \times 10^4$	-2 ± 4
	100	1.85	1.26 ± 0.38	$(4 \pm 3) \times 10^4$	-9 ± 9

2.2. Characterization of Polymer Field-Effect Transistors

To investigate the impact of mixed solvents on charge transport, we first measured the electronic performance of spin-coated PTDPPTFT4 FETs in an inert atmosphere. A summary of the measured results is compiled in **Table 1**. The charge carrier mobility was calculated from the slope of the square root of drain-to-source current ($I_{DS}{}^{1/2}$) versus gate voltage (V_g) in the

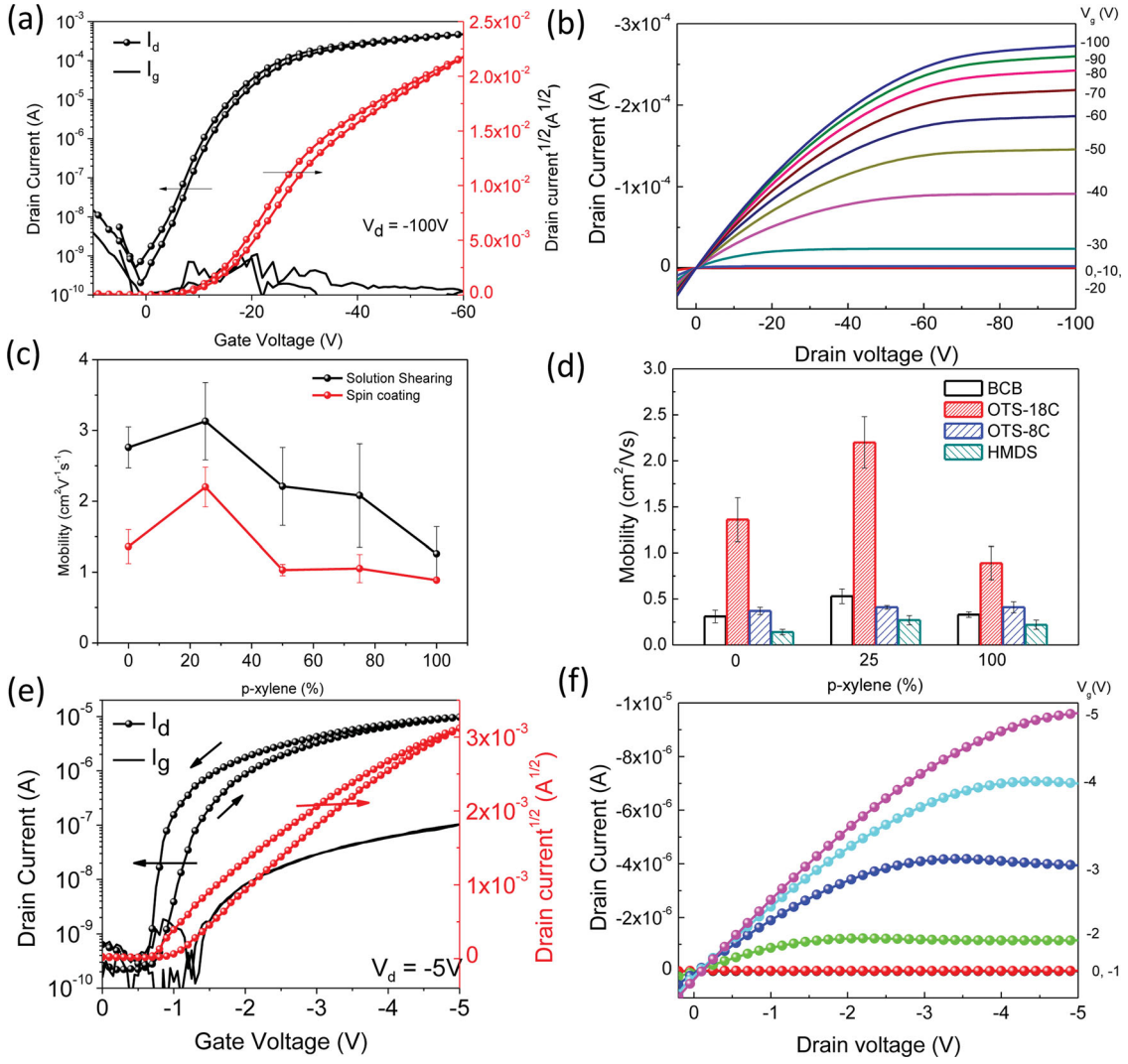

Figure 2. a) Transfer and b) output characteristics of solution-sheared PTDPPTFT4 FETs, where V_d = –100 V. c) Hole mobilities of the solution-sheared and spin-coated PTDPPTFT4 FETs as a function of mixed-solvent ratios. d) Hole mobilities of spin-coated PTDPPTFT4 on different surface. e) Transfer and f) output characteristics of spin-coated PTDPPTFT4 FETs on crosslinked PVP dielectrics, where V_d = –5 V.

saturation regime. The average mobilites were obtained from 5 to 13 devices for each condition. **Figure 2**a,b show the typical transfer and output electrical characteristics of a FET, respectively. All of the FETs fabricated on the octadecyltrimethoxylsilane (OTS)-modified SiO_2 dielectrics exhibited well-defined linear and saturation regimes. The transfer curve shows a hysteresis of less than 3 V, attributed to the good passivation of charge traps on the dielectric surface by the crystalline OTS self-assembled monolayer prepared according to our previously reported procedures.[40,41] As shown in Table 1 and Figure 2c, the PTDPPTFT4 FETs spin-coated from 0, 25, 50, 75, and 100% *p*-xylene solutions exhibited average hole mobilities of 1.36, 2.20, 1.03, 1.05 and 0.89 cm^2 V^{-1} s^{-1} respectively, indicating that the performance is sensitive to the selection of solvents. The spin-coated devices prepared from 25% *p*-xylene exhibited a maximum mobility of 2.53 cm^2 V^{-1} s^{-1}, on/off ratio of 2×10^6, and threshold voltage of –18 V. We also evaluated the mixed-solvent system on various surfaces, including polymer dielectrics, such as divinyltetramethylsiloxane-bis(benzocyclobutene) derivative (BCB) and crosslinked poly(4-vinyl phenol) (PVP) and SiO_2 dielectric modified with different self-assembly monolayers (hexamethyldisilazane (HMDS, contact angle: 80°), octyltrimethoxylsilane (OTS-C8, contact angle: 96°) and octadecyltrimethoxylsilane (OTS-C18, contact angle: 108°); as shown in Figure 2d). Even on different dielectrics, mixed-solvent devices prepared from 25% *p*-xylene still showed higher mobilities compared to single-solvent devices.

An OTS-modified crosslinked PVP dielectrics enable high-performance low-voltage devices. Figure 2e,f show the transfer and output curves of the FETs spin-coated from 25% *p*-xylene solution. These devices showed an average hole mobility of 1.38 cm^2 V^{-1} s^{-1} and a maximum mobility of 1.86 cm^2 V^{-1} s^{-1}, on/off ratio of 2×10^4, and threshold voltage of –1.2 V with a low saturation gate-source voltage of 5 V. The performance of PTDPPTFT4 spin-coated on a crystalline OTS-modified PVP surface is comparable to that on a 300 nm thick SiO_2 dielectric,

despite the operation voltage (5 V) of the PVP devices being much lower than that of the SiO_2 devices (100 V). Besides, we observe small hysteresis of ca. 0.5 V in PVP-based devices. The small hysteresis may be attributed to the moisture in the air. We note that the PVP-based devices were made and evaluated in ambient conditions. The moisture is easily to be absorbed by PVP due to its hydroxyl groups, and then results in the formation of defects at the semiconductor/dielectric interface. The hysteresis can be significantly reduced when measuring in an inert atmosphere. Although the devices were stored and evaluated in the air, the device still showed excellent stability. After storing in air for more than two months, the mobility and threshold voltage showed only a slight degradation (average mobility decreased from 1.38 to 1.15 $cm^2\ V^{-1}\ s^{-1}$ and the average threshold voltage only increased by 0.1 V) (Figure S2, Supporting Information). The excellent air stability is presumably due to the low HOMO level of PTDPPTFT4 (–5.3 eV), leading to good oxidation stability.

To further improve device performance, we used solution shearing to prepare polymer thin films. As shown in Table 1, the solution-sheared FETs from 0, 25, 50, 75, and 100% *p*-xylene solutions exhibited average hole mobilities of 2.76, 3.13, 2.21, 2.08, and 1.26 $cm^2\ V^1\ s^{-1}$ respectively. The solution-sheared devices made from 25% *p*-xylene again exhibited the highest maximum mobility of 3.94 $cm^2\ V^{-1}\ s^{-1}$. The improved performance obtained here compared to spin coating is due to the fine tuning of morphology using mixed solvents and the solution shearing method (see morphology characterization in Section 2.3.).

From the above device characterization, both of the spin-coated and solution sheared devices consistently showed a similar trend, the highest mobilities obtained from the 25% *p*-xylene solution. Several factors may contribute to this trend. One possible factor is the solvent evaporation rate. The use of a high boiling-point solvent may facilitate crystal growth and enhance charge transport. THN is a high boiling point solvent (b.p. of 208 °C). We observed that the THN-cast film (0% *p*-xylene) significantly increased evaporation time for spin coated films (>30 min for 0% *p*-xylene versus <1 min for 100% *p*-xylene). However, the solvent evaporation rate is insufficient to explain why the film cast from pure THN showed a lower mobility compared to that coated from the 25% *p*-xylene solution, which had a lower boiling point. Furthermore, during solution-shearing, we used an elevated substrate temperature somewhat below the boiling point of the solvent to better control the deposition rate. Higher temperatures caused faster deposition, thicker films and eventually lower device performance, while lower temperatures may prevent polymer film deposition on OTS-modified SiO_2 substrates. The optimized substrate temperatures of the solution-sheared films prepared from 0, 25, 50, 75, and 100% *p*-xylene are 145, 130, 117, 108, and 97 °C, respectively, and the drying time of each solution-sheared film was less than 1 minute, even using high boiling-point THN. Therefore, despite the short evaporation time with solution shearing, the mobilities of FETs made from solution shearing are still consistently higher than those prepared from spin coating, which experienced a longer deposition time. To further understand the impact of mixed solvents and solution shearing, we characterized the film surface morphology and crystalline structure, as discussed below.

2.3. Morphology Characterizations

To investigate the influence of mixed solvents on surface morphologies, the topographical images of the spin-coated and solution-sheared films (**Figures 3**,**4**) were obtained by atomic force microscopy (AFM). As shown in Figure 3, the spin-coated films prepared from the pure THN solution displayed a smooth surface. This may be attributed to the high solubility of the polymer in THN. With increasing proportions of *p*-xylene, larger aggregates and porous morphology were observed. The root-mean-square roughnesses increased for films made from 0, 25, 50, 75, and 100% *p*-xylene, with values of 2.1, 2.0, 2.2, 3.3, to 5.3 nm, respectively. This roughness trend may be attributed to increased aggregation formation by *p*-xylene.

The solution shearing method was previously reported by our group as an effective coating method to prepare crystalline films of small molecules and polymers.[31–33,42,43] Here, the solution-sheared film made from a THN solution displayed a morphology consisting of many small spherical aggregates (Figure 4a), while the film prepared from pure *p*-xylene revealed mesh-like features with many small bundles of nanofibers (Figure 4e). When mixing THN and *p*-xylene, the resulting thin-film surface morphology dramatically changed. The 50 and 75% *p*-xylene films showed mesh-like morphologies with many deep voids with a depth of 52 and 74 nm, respectively (Figure 4c,d). Similar mesh-like morphologies were also observed in spin-coated films made from *p*-xylene-rich solutions (75 and 100% *p*-xylene, Figure 3). As compared to 50 and 75% *p*-xylene films with the mesh-like morphology, the surface of the film prepared from a 25% *p*-xylene solution showed large bundles of nanofibers with shallower voids (depth = 25 nm) (Figure 4b). The changes in these surface morphologies may be attributed to the solubility behavior of polymer chains in solution, which we investigated using small angle X-ray scattering (see discussion in Section 2.4. below). Note that the deep grain boundaries are not desirable for charge transport, because it has been reported that the grain boundaries cause an energy barrier and limit charge carrier mobility in organic films.[23] Therefore, the mesh-like or porous morphologies may reduce charge transport in the films made with a large amount of *p*-xylene.

It has been shown that some polymer nanofibers have high crystallinity and good charge transport.[23] Intriguingly, nanofiber bundles were only observed in solution-sheared films rather than spin-coated films. There are several possible interpretations for these morphology differences. One possible reason is the influence of substrate temperatures. As compared to the spin coating technique, the solution shearing was performed at an elevated temperature. The high temperature may improve the solubility and aid the disentanglement of polymer chains in solution, resulting in better molecular packing. The second possible reason is the induced convection in solution shearing. During solution shearing, rapid solvent evaporation at the meniscus front induces a convective flow, which facilitates mass transport and may enhance crystal growth. Another possibility is improved molecular packing in the organic semiconductors. Previously, we have observed that solution shearing results in the formation of meta-stable strained packing structure of TIPS-pentacene and enhances π–π stacking.[31] Hence, different processing conditions may also lead to different

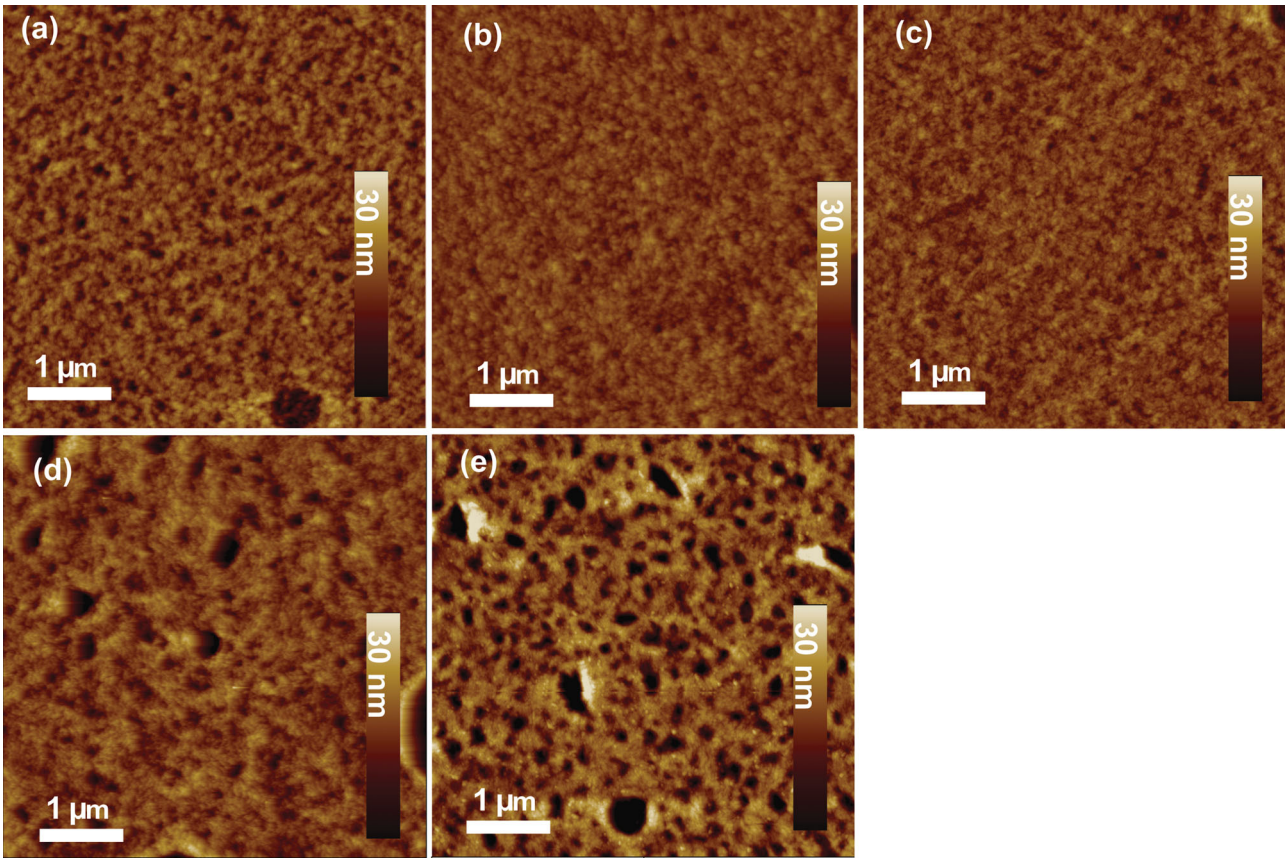

Figure 3. AFM topography images of spin-coated PTDPPTFT4 films made from different mixed-solvent ratios: THN with a) 0%, b) 25%, c) 50%, d) 75% *p*-xylene, and e) 100% *p*-xylene.

molecular packing in the polymer film. To gain a better understanding of the influence of mixed-solvent effects on the molecular packing, we employ X-ray diffraction to explore the aggregation behavior in solution and the crystalline structures of polymer in films (see Section 2.5.).

2.4. Solution Small Angle X-Ray Scattering

In the above UV-vis absorption section, we found that the higher content of *p*-xylene induces more aggregates in solution. However, the UV-vis spectra cannot provide much information about polymer conformation in solution. To investigate the aggregation behavior of our polymer in various solvents, we employed small angle X-ray scattering (SAXS), as shown in **Figure 5**, and analyzed the data with the Unified approach, which is a combination of Porod's and Guinier's law.[44] Guinier's law was used to estimate radius of gyration, R_g, which is a measure for the effective size of aggregates, as well as the sub-units within the aggregate.[44–47] Regardless of the solvent system, a high q Guinier regime (region iii) is observed. The model fitting in the high q Guinier regime shows that R_g steadily increases with increased *p*-xylene concentration, with R_g = 6.5, 7.3, 7.3, 9.8, and 10.3 Å for 0%, 25%, 50%, 75%, and 100% *p*-xylene respectively. We attribute the Guinier region observed in this high q region to arise from scattering from the monomer repeat unit, with the steady increase arising to the monomer repeat unit taking on a more expanded conformation. We believe it is likely that this expansion is due to the increased solubilizing of the side chains with increased *p*-xylene concentration.

In the intermediate q region, region ii from approximately 0.01 $Å^{-1}$ to 0.1 $Å^{-1}$, we observe a power law scaling which we fit to the Porod law. The Porod exponent provides insight into the geometrical conformation of the larger scale polymer aggregate. We expect a Porod exponent of –2 for a polymer which adopts a Guassian coil, while deviation to more negative Porod exponents indicates a collapsed coil conformation and deviation to less negative Porod exponents indicates an expanded coil conformation.[48] At the extreme of the expanded coil conformation a Porod exponent of –1 indicates that the aggregate has adopted a rigid rod structure.[48] For all cases observed here we observe Porod exponents very close to –1, with the 0%, 25%, 50%, 75% and 100% xylene samples exhibiting Porod exponents of –1.3, –1.1, –1, –1.3, and –1.2 respectively. This indicates that in the case of the 0%, 75%, and 100% *p*-xylene solutions, the polymer chains which comprise the aggregate have adopted an expanded coil conformation. However, at lower percentages of *p*-xylene (25% and 50%), the polymer chains are very stiff, indicating that the polymer chains have adopted a more rigid rod structure in solution.

Lastly, at the lowest q measured we observe a second Guinier plateau, region (i), for the 0%, 75% and 100% xylene samples,

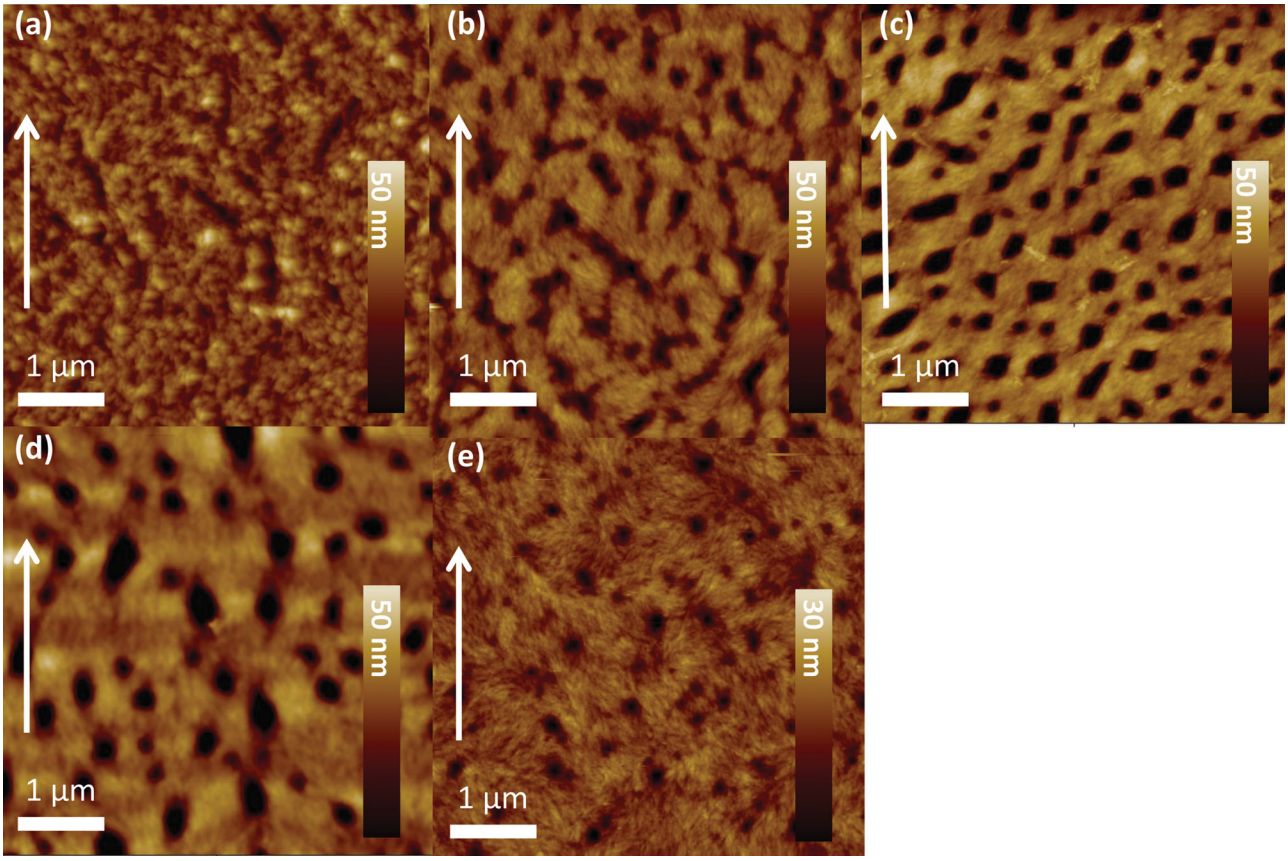

Figure 4. AFM topography images of solution-sheared PTDPPTFT4 films made from different mixed-solvent ratios at a shearing speed of 1 mm s^{-1}: THN with a) 0%, b) 25%, c) 50%, d) 75%, *p*-xylene, and e) 100% *p*-xylene.

with associated Rg of ≈ 30 nm, 16 nm, and 20 nm. For the 25 and 50% xylene samples, no second Guinier region is observed within our measurement range indicating that the solution phase aggregates are larger than 30 nm. The large size of these aggregates also indicates that these solution phase aggregates are comprised of multiple, loosely connected polymer chains, as the expected R_g for a single chain should be on the order of 10 nm for a completely rigid polymer coil and 4 nm for a polymer which adopts a Guassian coil conformation.[48,49] The fact that the Guinier region is not observed in the case of the 25% and 50% *p*-xylene solutions coupled to the observation of a decrease in the Porod exponent. The addition of lesser amounts of *p*-xylene most likely causes the polymer chains to fully elongate and adopt a rigid rod structure resulting in larger aggregates than when the individual chains are more collapsed as is the case in the pure THN solutions as well as when larger amounts of xylene is added.

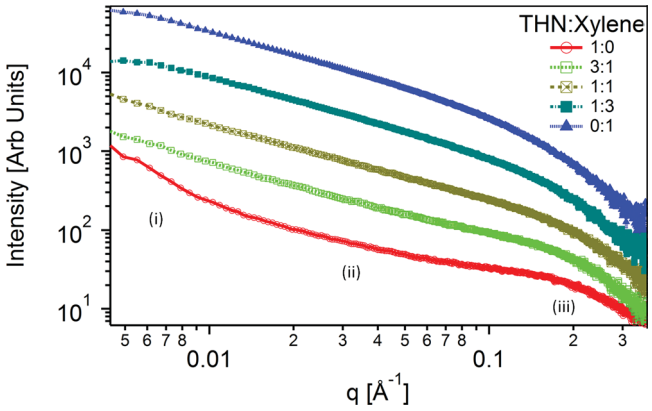

Figure 5. Small angle X-ray scattering curves for PTDPPTFT4 as a function of THN:*p*-xylene solvent ratio. Three regimes are present i) a guinier regime at the lowest *q* measured, ii) a porod regime at 0.01 >*q* > 0.1 $Å^{-1}$, and iii) a final guinier regime at high *q*.

The SAXS analysis reveals that a small amount of *p*-xylene significantly enhanced the stiffness of the individual polymer chains resulting in larger more extended solution phase aggregates. However, the further increase in *p*-xylene resulted in the side chains acting as the sole solubilizing groups, and the insufficient solvation of the side chains may lead to the collapse of the chains, potentially causing an increase of disorder within the aggregates.

2.5. Grazing-Incidence X-Ray Diffraction

The molecular packing of the PTDPPTFT4 films prepared on a crystalline octadecyltrimethoxylsilane (OTS-C18) -modified[41] bare Si substrate using solution shearing was investigated by grazing-incidence X-ray diffraction (GIXD) (**Figure 6**). PTDPPTFT4 showed well-defined high-order diffraction peaks

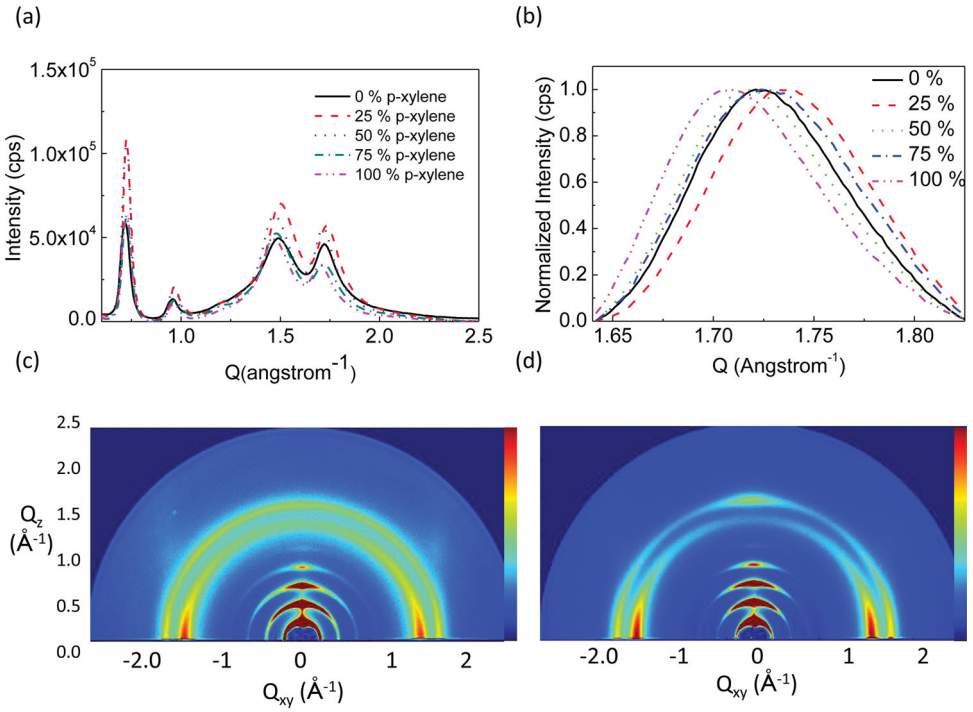

Figure 6. a) GIXD measurements for solution-sheared PTDPPTFT4 films. b) The (010) diffraction peaks of solution-sheared films. c,d) Two-dimensional GIXD patterns of c) 0% and d) 25% *p*-xylene films.

near the out-of-plane axis, which are due to an ordered lamellar structure. The calculated lamellar spacing of PTDPPTFT4 with two $C_{17}H_{35}$ side chains is 25.8 Å (**Table 2**), similar to the spacing of PBTTT with $C_{18}H_{37}$ side chains,[50] suggesting that PTDPPTFT4 may possess an inter-digitated packing of linear alkyl side chains or a tilted molecular plane. In addition, the PTDPPTFT4 film displayed two well-defined in-plane diffraction peak at 1.48 and 1.74 Å^{-1} (Figure 6a), which are attributed to an ordered packing of the side-chains and to ordered π–π stacking, respectively. The calculated spacing of the in-plane diffraction peaks at 1.48 Å^{-1} was 4.23 Å, which is the same as our previously reported peak position for the crystalline OTS monolayer with a hexagonal lattice.[40,41] However, this peak was still observed even if PTDPPTFT4 was spin coated on a bare Si substrate without any OTS modification (Figure S3, Supporting Information). Additionally, differential scanning calorimetry (DSC) showed a melting point of around 40–45 °C. Together, this evidence suggests the side chains of PTDPPTFT4 formed an ordered structures, rarely seen for other conjugated polymers.This peak is much stronger in the in-plane direction compared to the out-of-plane direction suggesting that the side-chains prefer an edge-on packing structure on the substrate (nearly upright standing and interdigitated).

Table 2. Grazing-incident X-ray diffraction data for PTDPPTFT4 FETs using different mixed-solvent ratios.

Process	*p*-Xylene (%)	Lamellar spacing [Å]	FWHM of out-of-plane peak[a)] [Å^{-1}]	π–π stacking distance [Å]
spin coating	0	25.7	0.062	3.70
	25	25.9	0.059	3.71
	50	25.8	0.060	3.70
	75	25.8	0.059	3.71
	100	25.8	0.057	3.72
solution shearing	0	26.1	0.045	3.64
	25	25.8	0.038	3.62
	50	25.8	0.041	3.66
	75	25.8	0.044	3.64
	100	25.8	0.045	3.68

The higher q in-plane peak at 1.74 Å^{-1} is attributed to π–π stacked packing between polymer chains. The π–π stacking peak position is calculated by summing the intensities along Chi from 0 to 82 degrees, between Q of 1.62 and 1.85 Å^{-1}, after background subtraction (Figure S4, Supporting Information). We note that this pi-pi stacking peak position is an average throughout the film. Figure 6b shows the π–π stacking peaks of films made from various mixing ratios. Intriguingly, we observed that π–π stacking distance slightly depended on the mixed solvent ratios when using solution shearing. The smallest π–π stacking distance (3.62 Å) was observed in the film made from 25% *p*-xylene. We observed that the π–π stacking distance of the solution-sheared film was smaller than that of equivalent films prepared from spin coating (3.71 Å) by almost 0.1 Å (Table 2). A smaller π–π stacking distance is expected to yield higher intermolecular overlap integral, beneficial to charge transport in the film.[9] Therefore, the solution sheared devices can show almost two times higher mobilities compared to spin coated devices. Furthermore, this close molecular packing partly explains why the nanofiber bundles were

observed only in solution-sheared films. Note that a change of molecular packing was observed in the solution-sheared films, indicating that solution shearing could be used to tune polymer packing structures. Further optimization of device performance of solution sheared devices based on polymer materials will be reported in due course.

The crystalline orientation of polymer films can be characterized by the intensity distribution of diffraction peaks.[51] Typically, more oriented films were found to have more efficient charge transport due to better alignment between adjacent ordered regions. However, some polymers showed high mobility with a mixture of face-on and edge-on orientations of the polymer backbones.[9] Figures 6c,d shows the GIXD pattern of solution-sheared films prepared from 0% and 25% *p*-xylene. The pure THN film (i.e., 0% *p*-xylene) showed more isotropic diffraction pattern than other films, indicating more random orientation of polymer chains in pure THN film. The more random orientation inferred from GIXD is consistent with the morphology of the THN film via AFM (Figure 3a). The film produced from a 25% *p*-xylene solution displayed a mixture of edge-on and face-on orientations. Furthermore, as compared with 0% *p*-xylene, there is an increasing fraction of edge on orientation. However, when deposited from solutions with a larger amount of *p*-xylene (50, 75, and 100%), the diffraction patterns of polymer films again became more isotropic (Figure S5, Supporting Information), indicating the crystalline domains became less orientated with larger amounts of *p*-xylene. The better crystalline orientation may be affected by either the high thickness or fast solvent evaporation. The film thickness typically increased with the increased *p*-xylene amount, presumably because *p*-xylene evaporates faster. As a result, the 100% *p*-xylene film exhibited the highest thickness (around 127 nm) among all polymer films. Himmelberger and coworkers previously investigated the effects of confined thin film geometry on polymer crystallization behavior.[52] They found that a thinner polymer film gave a more oriented crystalline film than a thicker film due to the confinement effect and influence by the semiconductor/substrate and semiconductor/solvent interfaces. Since the confinement effect decreases in the thicker films, the films became less oriented in the PTDPPTFT4 films made with a higher content of *p*-xylene. In addition to the thickness effects, the lower boiling point of *p*-xylene, compared to THN, may cause faster film deposition and induce more defects embedded in polymer films. As discussed above, using a small amount of *p*-xylene can facilitate closer molecular packing and more oriented films. On the other hand, the use of large amount of *p*-xylene induced more isotropic films, possibly limiting charge transport. Therefore, the combination of the mixed-solvent approach and solution shearing can be used to tune the thin film packing and morphology of conjugated polymers.

3. Conclusion

High-performance solution-sheared polymer thin-film transistors processed through non-chlorinated mixed solvents have been demonstrated. The charge transport, crystalline orientation and film morphology of the polymer devices were all observed to be significantly affected by changing the ratios of *p*-xylene to THN in the mixed solvent systems. When the amount of *p*-xylene was increased in the mixed solvent, a higher degree of aggregation along with a more oriented film was obtained with the polymer backbone edge-on on the substrate. In contrast, an increase in the amount of THN resulted in a slower evaporation rate (due to its higher boiling point), hence providing a longer deposition time to allow for ordered molecular assembly. By optimizing the ratio of mixed solvents, we observed that the performance of FETs are vastly improved with both spin coating and solution shearing. It was also observed that the stiffness of polymer aggregates increased in solution upon the addition of a small amount of *p*-xylene, thus resulting in the formation of highly crystalline nanofibers. When mixing with a small amount of *p*-xylene, the PTDPPTFT4 films exhibited closer molecular packing and better crystalline orientation. For PTDPPTFT4 FETs prepared via the solution shearing approach, the resulting highly aligned crystalline nanofiber bundles showed a mobility as high as 3.94 $cm^2\ V^{-1}\ s^{-1}$. PTDPPTFT4 also exhibited a mobility more than 1 $cm^2\ V^1\ s^{-1}$ at a low voltage of 5 V on the crosslinked poly(4-vinylphenol) (PVP) dielectric layer. Furthermore, our fabricated device showed prolonged air stability, even after exposure to air for two months. In summary, this study demonstrates that using carefully identified non-chlorinated mixed solvents and a coplanar donor-acceptor polymer can collectively provide a promising path forward for practical organic electronics applications.

4. Experimental Section

Characterization: Tapping-mode AFM images of the films were recorded using a Multimode Nanoscope III with Extender electronics (Digital Instruments/Veeco Metrology Group, Santa Barbara, CA). UV-vis spectra were measured with a Varian Cary 6000i UV-vis. spectrophotometer. The capacitance of the polymer dielectric layer was recorded using an Agilent E4980A LCR meter. Transmission SAXS studies on the casting solutions were carried out at beamline 4–2 at the Stanford Synchrotron Radiation Light source. It is noteworthy that the solution SAXS was performed at an elevated temperature around 75 °C to prevent polymer gelation, which blocks the transfer of polymer solution. Grazing incidence X-ray diffraction (GIXD) patterns were measured at the Stanford Synchrotron Radiation Lightsource on beamline 11–3 with a photon energy of 12.73 keV. The angle of incidence was fixed at 0.12° to enhance the diffraction intensity and reduce substrate scattering. Numerical integration of the diffraction peak areas was performed with the software WxDiff.[53]

Transistor Fabrication: Highly doped *n*-type Si (100) wafers (<0.004 Ω cm) were used as substrates. A 300 nm SiO_2 layer (capacitance per unit area C_i = 10 $nFcm^{-2}$) was thermally grown onto the Si substrates as a gate dielectric. These wafers were cleaned by using oxygen plasma (Jelight Inc. UVO-Cleaner 42) at a power of 150 W under oxygen pressure of 200 Torr for 5 min. Crystalline octadecyltrimethoxylsilane (OTS)-treated surface on SiO_2/Si substrates were obtained by the following procedures: a clean SiO_2/Si substrate was spin-coated with a solution of 3 mM OTS solution in trichloroethylene (TCE), and then the substrates were treated overnight with an ammonia vapor.[40,41] The OTS-treated surface was rinsed with toluene, acetone and isopropyl alcohol, and then dried with nitrogen. The contact angle of the OTS-treated SiO_2/Si substrates, measured with deionized water, was approximately 108°. The organic semiconductor thin films were deposited on SiO_2/Si substrates through solution-shearing (SS) or spin-coated methods. The polymer solution was heated at 120 °C

so that the solution would be fully dissolved prior to solution processing. Solution-sheared thin films were prepared as reported previously.[26] The optimized substrate temperatures for solution shearing are significantly below the boiling points of the solvents.[32] In our mixed-solvent system, the substrate temperatures range from 97 °C to 145 °C, depending on the ratio of mixed solvents. The drying time of all solution-sheared films was less than 1 min even using high boil-point THN, because of applied substrate temperatures. In contrast, the spin-coated films using THN as a solvent commonly take at least half an hour to completely dry. The solution concentrations for spin coating and SS deposition ranged from 2–10 mg mL^{-1}. The spin-coated films were deposited from the mixed-solvent solution (*p*-xylene/THN) at a spin rate of 1000 rpm for 60 s, and the SS films were prepared at a shearing rate of 0.2–4 mm s^{-1}. The film thicknesses of these solution-sheared and spin-coated films range from 48 nm to 127 nm. To obtain high crystallinity, these samples were annealed at 190 °C for an hour in inert atmosphere. Gold contacts (40 nm) were evaporated onto the SS and spin-coated thin films with a channel length (L) of 50 μm, and a channel width (w) of 1000 μm. The polymer dielectric layer was prepared by spin coating a solution of poly(vinyl phenol) (PVP) (Sigma-Aldrich, Mw around 25 000) and 4,4′-(hexafluoro-isopropylidene) diphthalic anhydride (HDA) (Sigma-Aldrich, 99%) with a ratio of 10:1 (PVP:HDA) in propylene glycol monomethyl ether acetate (PGMEA). The concentration of the combined PVP and HDA in solution was 40 mg mL^{-1}. Triethlyamine (Sigma-Aldrich, 99%) was used as a catalyst. Spin-coating rate was 7000 rpm for 60 s.[54] The dielectric layer was annealed at 120 °C for at least 2 h for crosslinking, and then a second layer was spin-coated on the dielectric layer and annealed again (final PVP thickness = 45 nm).[55] The FET transfer and output characteristics were recorded in a N_2-filled glove box or in air by using a Keithley 4200 semiconductor parametric analyzer (Keithley Instruments, Cleveland, OH).

Supporting Information

Supporting Information is available from the Wiley Online Library or from the author.

Acknowledgements

The authors acknowledge funding support from the National Science Foundation DMR Solid State Chemistry (DMR-DMR-1303178) and Corning Corporation. W.-Y.L. acknowledges postdoctoral fellowship support from Postdoctoral Research Abroad Program sponsored by the National Science Council, Taiwan. S.C.B.M. and Y.D. acknowledge support by the Department of Energy, Laboratory Directed Research and Development funding, under contract DE-AC02–76SF00515. . Portions of this research were carried out at the Stanford Synchrotron Radiation Lightsource, a Directorate of SLAC National Accelerator Laboratory and an Office of Science User Facility operated for the U.S. Department of Energy Office of Science by Stanford University. The beamline 4–2 is part of the SSRL Structural Molecular Biology Program which is supported by the DOE Office of Biological and Environmental Research, and by the National Institutes of Health, National Institute of General Medical Sciences (including P41GM103393) and the National Center for Research Resources (P41RR001209).

Received: November 8, 2013
Revised: December 16, 2013
Published online: March 3, 2014

[1] J. Zaumseil, H. Sirringhaus, *Chem. Rev.* **2007**, *107*, 1296.
[2] (Eds: Z. Bao, J. Locklin), Organic field-effect transistors, CRC press, Boca Raton, FL **2007**.
[3] A. C. Arias, J. D. MacKenzie, I. McCulloch, J. Rivnay, A. Salleo, *Chem. Rev.* **2010**, *110*, 3.
[4] Z. Bao, A. Dodabalapur, A. J. Lovinger, *Appl. Phys. Lett.* **1996**, *69*, 4108.
[5] L. H. Jimison, M. F. Toney, I. McCulloch, M. Heeney, A. Salleo, *Adv. Mater.* **2009**, *21*, 1568.
[6] B. H. Hamadani, D. J. Gundlach, I. McCulloch, M. Heeney, *Appl. Phys. Lett.* **2007**, *91*, 243512.
[7] H. N. Tsao, D. M. Cho, I. Park, M. R. Hansen, A. Mavrinskiy, D. Y. Yoon, R. Graf, W. Pisula, H. W. Spiess, K. Müllen, *J. Am. Chem. Soc.* **2011**, *133*, 2605.
[8] S. Wang, M. Kappl, I. Liebewirth, M. Müller, K. Kirchhoff, W. Pisula, K. Müllen, *Adv. Mater.* **2012**, *24*, 417.
[9] J. Mei, D. H. Kim, A. L. Ayzner, M. F. Toney, Z. Bao, *J. Am. Chem. Soc.* **2011**, *133*, 20130.
[10] T. Lei, J.-H. Dou, Z.-J. Ma, C.-H. Yao, C.-J. Liu, J.-Y. Wang, J. Pei, *J. Am. Chem. Soc.* **2012**, *134*, 20025.
[11] Y. Li, S. P. Singh, P. Sonar, *Adv. Mater.* **2010**, *22*, 4862.
[12] J. Li, Y. Zhao, H. S. Tan, Y. Guo, C.-A. Di, G. Yu, Y. Liu, M. Lin, S. H. Lim, Y. Zhou, H. Su, B. S. Ong, *Sci. Rep.* **2012**, *2*, 754.
[13] H.-W. Lin, W.-Y. Lee, W.-C. Chen, *J. Mater. Chem.* **2012**, *22*, 2120.
[14] I. Kang, T. K. An, J.-a. Hong, H.-J. Yun, R. Kim, D. S. Chung, C. E. Park, Y.-H. Kim, S.-K. Kwon, *Adv. Mater.* **2013**, *25*, 524.
[15] Z. Yi, X. Sun, Y. Zhao, Y. Guo, X. Chen, J. Qin, G. Yu, Y. Liu, *Chem. Mater.* **2012**, *24*, 4350.
[16] C. Kanimozhi, N. Yaacobi-Gross, K. W. Chou, A. Amassian, T. D. Anthopoulos, S. Patil, *J. Am. Chem. Soc.* **2012**, *134*, 16532.
[17] J. Lee, A. R. Han, J. Kim, Y. Kim, J. H. Oh, C. Yang, *J. Am. Chem. Soc.* **2012**, *134*, 20713.
[18] H. Chen, Y. Guo, G. Yu, Y. Zhao, J. Zhang, D. Gao, H. Liu, Y. Liu, *Adv. Mater.* **2012**, *24*, 4589.
[19] J. S. Ha, K. H. Kim, D. H. Choi, *J. Am. Chem. Soc.* **2011**, *133*, 10364.
[20] H. Bronstein, Z. Chen, R. S. Ashraf, W. Zhang, J. Du, J. R. Durrant, P. Shakya Tuladhar, K. Song, S. E. Watkins, Y. Geerts, M. M. Wienk, R. A. J. Janssen, T. Anthopoulos, H. Sirringhaus, M. Heeney, I. McCulloch, *J. Am. Chem. Soc.* **2011**, *133*, 3272.
[21] W. M. Zhang, J. Smith, S. E. Watkins, R. Gysel, M. McGehee, A. Salleo, J. Kirkpatrick, S. Ashraf, T. Anthopoulos, M. Heeney, I. McCulloch, *J. Am. Chem. Soc.* **2010**, *132*, 11437.
[22] J.-F. Chang, B. Sun, D. W. Breiby, M. M. Nielsen, T. I. Sölling, M. Giles, I. McCulloch, H. Sirringhaus, *Chem. Mater.* **2004**, *16*, 4772.
[23] H. Yang, T. J. Shin, L. Yang, K. Cho, C. Y. Ryu, Z. Bao, *Adv. Funct. Mater.* **2005**, *15*, 671.
[24] Y. D. Park, H. S. Lee, Y. J. Choi, D. Kwak, J. H. Cho, S. Lee, K. Cho, *Adv. Funct. Mater.* **2009**, *19*, 1200.
[25] L. Qiu, X. Wang, W. H. Lee, J. A. Lim, J. S. Kim, D. Kwak, K. Cho, *Chem. Mater.* **2009**, *21*, 4380.
[26] H. Li, B. C. K. Tee, J. J. Cha, Y. Cui, J. W. Chung, S. Y. Lee, Z. Bao, *J. Am. Chem. Soc.* **2012**, *134*, 2760.
[27] H. Li, B. C. K. Tee, G. Giri, J. W. Chung, S. Y. Lee, Z. Bao, *Adv. Mater.* **2012**, *24*, 2588.
[28] F. Zhang, C.-a. Di, N. Berdunov, Y. Hu, Y. Hu, X. Gao, Q. Meng, H. Sirringhaus, D. Zhu, *Adv. Mater.* **2013**, *25*, 1370.
[29] W. Pisula, A. Menon, M. Stepputat, I. Lieberwirth, U. Kolb, A. Tracz, H. Sirringhaus, T. Pakula, K. Mullen, *Adv. Mater.* **2005**, *17*, 684.
[30] H. A. Becerril, M. E. Roberts, Z. Liu, J. Locklin, Z. Bao, *Adv. Mater.* **2008**, *20*, 2588.
[31] G. Giri, E. Verploegen, S. C. B. Mannsfeld, S. Atahan-Evrenk, D. H. Kim, S. Y. Lee, H. A. Becerril, A. Aspuru-Guzik, M. F. Toney, Z. Bao, *Nature* **2011**, *480*, 504.
[32] W.-Y. Lee, J. H. Oh, S.-L. Suraru, W.-C. Chen, F. Würthner, Z. Bao, *Adv. Funct. Mater.* **2011**, *21*, 4173.
[33] J. H. Oh, W.-Y. Lee, T. Noe, W.-C. Chen, M. Könemann, Z. Bao, *J. Am. Chem. Soc.* **2011**, *133*, 4204.

[34] J. Lee, A. R. Han, J. Hong, J. H. Seo, J. H. Oh, C. Yang, *Adv. Funct. Mater.* **2012**, *22*, 4128.
[35] Y. Diao, B. C. K. Tee, G. Giri, J. Xu, D. H. Kim, H. A. Becerril, R. M. Stoltenberg, T. H. Lee, G. Xue, S. C. B. Mannsfeld, Z. Bao, *Nat. Mater.* **2013**, *12*, 665.
[36] J. R. Matthews, W. Niu, A. Tandia, A. Wallace, J. Hu, W.-Y. Lee, G. Giri, S. C. B. Mannsfeld, Y. Xie, S. Cai, H. H. Fong, Z. Bao, M. He, *Chem. Mater.* **2013**, *25*, 782.
[37] M. Koppe, C. J. Brabec, S. Heiml, A. Schausberger, W. Duffy, M. Heeney, I. McCulloch, *Macromolecules* **2009**, *42*, 4661.
[38] F. Machui, S. Abbott, D. Waller, M. Koppe, C. J. Brabec, *Macromol. Chem. Phys.* **2011**, *212*, 2159.
[39] B. Walker, A. Tamayo, D. T. Duong, X.-D. Dang, C. Kim, J. Granstrom, T.-Q. Nguyen, *Adv. Energy Mater.* **2011**, *1*, 221.
[40] A. Virkar, S. Mannsfeld, J. H. Oh, M. F. Toney, Y. H. Tan, G.-y. Liu, J. C. Scott, R. Miller, Z. Bao, *Adv. Funct. Mater.* **2009**, *19*, 1962.
[41] Y. Ito, A. A. Virkar, S. Mannsfeld, J. H. Oh, M. Toney, J. Locklin, Z. Bao, *J. Am. Chem. Soc.* **2009**, *131*, 9396.
[42] H. A. Becerril, N. Miyaki, M. L. Tang, R. Mondal, Y.-S. Sun, A. C. Mayer, J. E. Parmer, M. D. McGehee, Z. Bao, *J. Mater. Chem.* **2009**, *19*, 591.
[43] Y. Diao, B. C. K. Tee, G. Giri, J. Xu, D. H. Kim, H. A. Becerril, R. M. Stoltenberg, T. H. Lee, G. Xue, S. C. B. Mannsfeld, Z. Bao, *Nat. Mater.* **2013***12* , 665.
[44] B. Hammouda, *J. Appl. Crystallogr.* **2010**, *43*, 716.
[45] G. Beaucage, *J. Appl. Crystallogr.* **1996**, *29*, 134.
[46] G. Beaucage, *J. Appl. Crystallogr.* **1995**, *28*, 717.
[47] A. Guinier, G. Fournet, C. B. Walker, G. H. Vineyard, *Phys. Today* **1956**, *9*, 38.
[48] R.-J. Roe, Methods of X-ray and neutron scattering in polymer science, Oxford Univ. Press, New York, USA **2000**.
[49] P. J. Flory, Principles of Polymer Chemistry, Cornell University, USA **1953**.
[50] R. J. Kline, D. M. DeLongchamp, D. A. Fischer, E. K. Lin, L. J. Richter, M. L. Chabinyc, M. F. Toney, M. Heeney, I. McCulloch, *Macromolecules* **2007**, *40*, 7960.
[51] J. Rivnay, S. C. B. Mannsfeld, C. E. Miller, A. Salleo, M. F. Toney, *Chem. Rev.* **2012**, *112*, 5488.
[52] S. Himmelberger, J. Dacuña, J. Rivnay, L. H. Jimison, T. McCarthy-Ward, M. Heeney, I. McCulloch, M. F. Toney, A. Salleo, *Adv. Funct. Mater.* **2013**, *23*, 2091.
[53] S. C. B. Mannsfeld, M. L. Tang, Z. Bao, *Adv. Mater.* **2011**, *23*, 127.
[54] M. E. Roberts, N. r. Queraltó, S. C. B. Mannsfeld, B. N. Reinecke, W. Knoll, Z. Bao, *Chem. Mater.* **2009**, *21*, 2292.
[55] Z. Liu, J. H. Oh, M. E. Roberts, P. Wei, B. C. Paul, M. Okajima, Y. Nishi, Z. Bao, *Appl. Phys. Lett.* **2009**, *94*, 203301.